Tuning of the Metal–Insulator Transition in Nd-Doped Bilayer Nickelate $La_3Ni_2O_7$ Thin Films

Fang-Hui Zhu(朱芳慧)[1], Xue-Yan Wang(王雪妍)[1], Ting-Na Shao(邵婷娜)[2*], Qiang Zhao(赵强)[1], Wen-Long Yang(杨文龙)[1], Cheng-Xue Chen(陈承雪)[1], Mei-Ling Yan(严媚玲)[1], Rui-Fen Dou(窦瑞芬)[1,3], Chang-Min Xiong(熊昌民)[1,3*], and Jia-Cai Nie(聂家财)[1,3*]

[1]*School of Physics and Astronomy, Beijing Normal University, Beijing 100875, China*
[2]*Institute of System Engineering, AMS, PLA, Beijing 100020, China*
[3]*Key Laboratory of Multiscale Spin Physics, Ministry of Education, Beijing Normal University, Beijing 100875, China*

(Received 21 March 2025; accepted manuscript online 6 May 2025)

Recent studies have successfully demonstrated high-T_c superconductivity in bilayer nickelate $La_3Ni_2O_7$. However, research on modulating the structural and transport characteristics of $La_3Ni_2O_7$ films by applying "chemical" compressive pressure through cation substitution is still limited. Here, we address this issue in the $La_{3-x}Nd_xNi_2O_7$ ($x = 0$, 1.0, 1.5, 2.0, and 2.5) thin film samples. It was found that using Nd^{3+} with a smaller radius instead of La^{3+} can reduce the c-axis lattice constant and shift the metal–insulator transition (MIT) temperature T_{MIT}. To probe the origin of the MIT at cryogenic temperatures, experimental measurements of magnetoresistance were conducted, and theoretical analysis was carried out using the Kondo model, Hikami–Larkin–Nagaoka equation, and other methods. The results indicate that as Nd doping rises, the contributions of the Kondo effect and two-dimensional weak localization (WL) first decrease and then increase. The total contribution of WL and the Kondo effect in the mid-doped $La_{1.5}Nd_{1.5}Ni_2O_7$ sample was the smallest, which to some extent explains the changes in T_{MIT}. The Kondo effect dominates in other $La_{3-x}Nd_xNi_2O_7$ ($x = 0$, 1.0, 2.0, and 2.5) samples. This work demonstrates that cation doping has a significant impact on bilayer nickelates, providing experimental evidence for understanding the physical mechanism of the MIT in bilayer nickelates.

DOI: 10.1088/0256-307X/42/6/067303 CSTR: 32039.14.0256-307X.42.6.067303

1. Introduction. The breakthrough discovery of high-T_c superconductivity in cuprates[1] has stimulated significant interest in investigating nickelates with electronic properties and crystal structures analogous to those of cuprates.[2,3] In 2019, Li *et al.* discovered superconductivity ($T_c \approx 9$–15 K) in $Nd_{1-x}Sr_xNiO_2$ thin films.[4] Afterward, superconductivity was also discovered in $Pr_{1-x}Sr_xNiO_2$ and $La_{1-x}Sr_xNiO_2$ thin films.[5–7] In addition to the infinite-layer thin films, signatures of superconductivity have also been discovered in the quintuple-layer $Nd_6Ni_5O_{12}$ thin films, without chemical doping.[8] However, the superconductivity of nickelates is still limited to thin films, and there has been no progress in bulk superconductors for a long time.[9–11]

Recent experimental report has shown that Ruddlesden–Popper (RP) bilayer nickelate single crystal $La_3Ni_2O_7$ achieves high-temperature superconductivity ($T_c \approx 80$ K) under high-pressure conditions exceeding 14 GPa.[12] Transport and magnetic measurements of pressurized $La_3Ni_2O_7$ revealed the emergence of zero-resistance state and Meissner effect in both monocrystalline and polycrystalline specimens, constituting definitive proof of bulk superconductivity in this nickelate system.[13–16] To avoid the presence of 1313-polymorph and impurity RP phases, Wang *et al.* synthesized Pr-doped $La_2PrNi_2O_7$ polycrystalline samples and discovered that the superconducting transition temperature reaches $T_c^{onset} = 82.5$ K and $T_c^{zero} = 60$ K at 18–20 GPa.[17] In addition, signatures of superconductivity have also been observed in trilayer nickelate bulk (polycrystalline and single-crystalline) $La_4Ni_3O_{10}$ under high pressures.[18–22]

High pressure caused a structural phase transition, a slight reduction in the lattice parameters, and induced superconductivity in $La_3Ni_2O_7$.[12] This transition renders the Ni-O-Ni bond collinear, which may enhance electron hopping and possibly quash density waves that rival superconductivity.[23–25] Unlike a previous report,[26] $La_3Ni_2O_7$ thin film grown on a single crystal (00l)-oriented $LaAlO_3$ substrate successfully achieved a metal–insulator transition (MIT) with a transition temperature as low as 24.3 K.[27] Recently, high-temperature superconductivity has been successively achieved in $La_3Ni_2O_7$ and $La_{2.85}Pr_{0.15}Ni_2O_7$ thin films by applying compressive substrate strain and adopting the optimal growth and annealing conditions.[28,29] However, it has not been reported whether the properties of the film can be changed by applying "chemical" pressure via cation substitution.

In this letter, we report the successful fabrication of $La_{3-x}Nd_xNi_2O_7$ ($x = 0$, 1.0, 1.5, 2.0, and 2.5) thin films by pulsed laser deposition (PLD). Nd^{3+} with a smaller

*Corresponding author. Email: nana675@126.com; cmxiong@bnu.edu.cn; jcnie@bnu.edu.cn
© 2025 Chinese Physical Society and IOP Publishing Ltd. All rights, including for text and data mining, AI training, and similar technologies, are reserved.

radius was used to partially replace La^{3+} to apply chemical compressive stress to the thin films, which leads to a reduced MIT temperature (T_{MIT}) compared to the undoped $La_3Ni_2O_7$. $\ln T$ dependence of resistivity and negative magnetoresistance (MR) were observed at low temperatures. The temperature-dependent resistivity $\rho(T)$ and negative MR were successfully simulated using the Kondo model, Hikami–Larkin-Nagaoka (HLN) fitting, and other methods, with dominant physical mechanisms identified as the Kondo effect and weak localization (WL). For the mid-doped $La_{1.5}Nd_{1.5}Ni_2O_7$ sample, the total contribution of WL and the Kondo effect was the smallest, which may be the reason for the minimum T_{MIT}, while the WL contribution is slightly higher than that of the Kondo effect. The Kondo effect dominates in other $La_{3-x}Nd_xNi_2O_7$ ($x = 0$, 1.0, 2.0, and 2.5) samples.

2. Experiments. $La_{3-x}Nd_xNi_2O_7$ ($x = 0$, 1.0, 1.5, 2.0, and 2.5) target materials were synthesized through solid-state reactions in a muffle furnace. To begin with, a homogeneous mixture was prepared by thoroughly grinding La_2O_3, Nd_2O_3 and NiO powder in specific molar ratios using an agate mortar. Subsequently, the homogeneous powder mixture was calcined in a muffle furnace at 1200 ℃ for 24 hours, followed by cold pressing at 2 kbar into pellet form. Finally, the compacted powder was reheated to 1300 ℃ for 24 hours to obtain different doping target materials.

Using PLD technology, we fabricated a series of epitaxial $La_{3-x}Nd_xNi_2O_7$ ($x = 0$, 1.0, 1.5, 2.0, and 2.5) thin films on (100)-oriented $LaAlO_3$ (LAO) substrates. The deposition process maintained a substrate temperature of 620 ℃ while regulating oxygen pressure within 350–420 mTorr. The laser parameters were set to a 4 Hz pulse frequency with a 1.4 J/cm^2 energy density. The as-deposited films underwent post-growth annealing for 15 minutes followed by controlled cooling, with the deposition oxygen pressure maintained throughout the entire thermal treatment process.

Phase identification was performed with a Shimadzu X-ray diffractometer (XRD). The XRD patterns of different doped targets are shown in Fig. S1(a) of the Supplementary Materials (SM). The crystal orientation and thickness of the film samples were determined by XRD, as shown in Figs. S1(b) and S2 of the SM. The resistivity and MR measurements were carried out by a physical property measurement system (PPMS, Quantum Design). For precise transport property determination, we employed the Van der Pauw contact geometry. [30]

3. Results and Discussion. For a thin epitaxial film, it has been shown that the misfit strain could be coherently maintained during the film growth. [28,29,31] The XRD patterns of the $La_{3-x}Nd_xNi_2O_7$ films ($x = 0$, 1.0, 1.5, 2.0, and 2.5) are presented in Fig. S1(b) of SM. For all samples with a thickness of approximately 15 nm, the absence of (008) and (0014) peaks is due to the thinness of the samples. For the 24-nm-thick film, all the (00l) (l is even) peaks appear (see Fig. S2 of SM), indicating that we have achieved the fabrication of bilayer $La_{3-x}Nd_xNi_2O_7$ thin films with

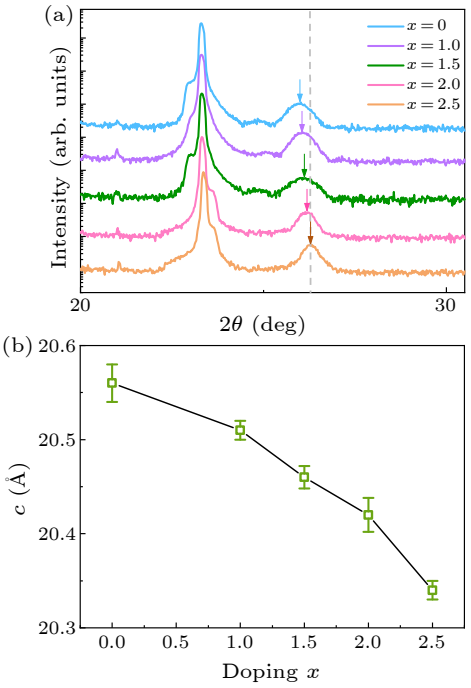

Fig. 1. (a) XRD patterns for (006) peaks of 15 nm thick $La_{3-x}Nd_xNi_2O_7$ ($x = 0$, 1.0, 1.5, 2.0, and 2.5) thin films grown on (100) $LaAlO_3$ substrates. The gray dashed line coincides with the (006) peak angle of the $La_{0.5}Nd_{2.5}Ni_2O_7$ sample. (b) Dependence of the c-axis lattice parameter on Nd-doping concentration. Error bars represent sample-to-sample variation.

excellent crystalline quality. With the rise in Nd doping concentration, the angle of the (006) diffraction peak increases slightly, as depicted in Fig. 1(a). Figure 1(b) reveals a contraction of the c-axis lattice parameter with progressive Nd substitution in the 15 nm thick film series. This demonstrates that it is achievable to apply compressive strain to the $La_3Ni_2O_7$ thin films by replacing a portion of La^{3+} with smaller radius Nd^{3+}.

The resistivity and T_{MIT} of films exhibit strong thickness-dependent variations, as shown in Fig. 2. It can be clearly seen from Fig. 2(b) that the $La_{1.5}Nd_{1.5}Ni_2O_7$ film with the lowest thickness (∼9 nm) shows the highest T_{MIT}. The enhanced surface scattering in thinner films can generate stronger scattering effects, [32] which may lead to the highest T_{MIT}. Figure 2(b) demonstrates a monotonic enhancement of the T_{MIT} with increasing film thickness above the critical threshold of 15 nm. It can be understood as follows: At ambient pressure, $La_3Ni_2O_7$ adopts the orthorhombic *Amam* space group ($a = 5.3928$ Å, $b = 5.4486$ Å, $c = 20.5185$ Å), [33,34] with an average in-plane pseudo-tetragonal parameter of ≈ 3.833 Å. The lattice parameter of the LAO substrate is 3.792 Å; therefore, the compressive misfit generated by LAO is about 1.0812%. As a consequence, the occurrence of misfit dislocations in the thicker film could account for the elevated T_{MIT}, considering that it is well-documented that oxygen vacancies tend to congregate at the dislocation's tensile region. [35,36] For subsequent experiments, we chose the samples with a fixed thickness of 15 nm.

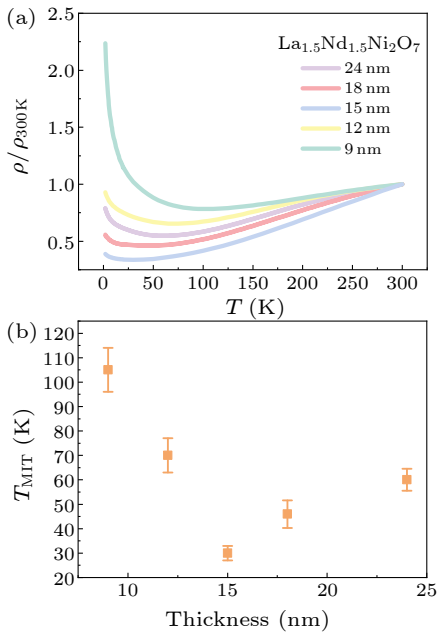

Fig. 2. (a) Normalized resistivity vs. temperature for $La_{1.5}Nd_{1.5}Ni_2O_7$ thin films with thickness of 9, 12, 15, 18 and 24 nm, respectively. (b) The variation of T_{MIT} with film thickness. Error bars represent sample-to-sample variation.

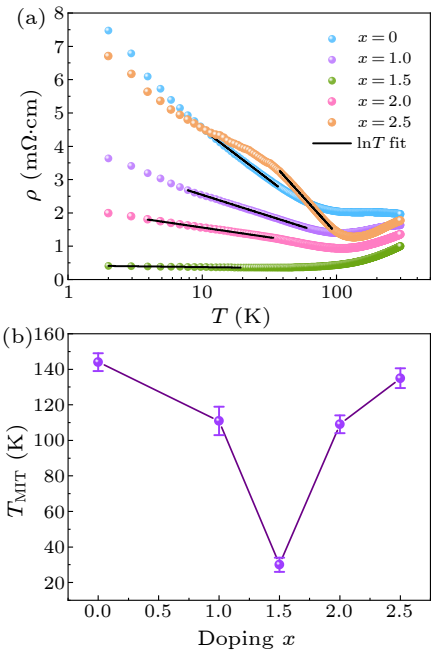

Fig. 3. (a) ρ–T curves of $La_{3-x}Nd_xNi_2O_7$ (x = 0, 1.0, 1.5, 2.0, 2.5) films. The black solid lines are the corresponding ln$T$ fits. (b) The variation of T_{MIT} with the Nd doping concentration x. Error bars represent sample-to-sample variation.

MIT is observed in all $La_{3-x}Nd_xNi_2O_7$ thin films (x = 0, 1.0, 1.5, 2.0, and 2.5). There are significant differences in T_{MIT} among different samples, as shown in Fig. 3(b). For the pristine $La_3Ni_2O_7$, T_{MIT} is about 144 K. With the increase in Nd doping levels, the T_{MIT} of the film progressively decreases, reaching the lowest value ($T_{MIT} \approx 29$ K) for mid-doped $La_{1.5}Nd_{1.5}Ni_2O_7$. Initially, the T_{MIT} reduction correlates with c-axis compression under epitaxial stress, which shortens Ni–Ni bonds and promotes metallic behavior, in qualitative agreement with prior studies.[37,38] Afterwards, further doping of Nd resulted in an increase in T_{MIT}. While chemical pressure induces lattice contraction similarly to physical pressure, it simultaneously generates anisotropic lattice distortion due to disparate responses along a-axis and b-axis.[39] The overall lattice compression resembles that induced by external hydrostatic pressure; the orthogonal lattice distortion results in significant enhancement of T_{MIT}. Consequently, excessive substitution of La^{3+} by smaller Nd^{3+} in $La_{3-x}Nd_xNi_2O_7$ induces significant lattice distortion due to the ionic radius mismatch, thereby increasing resistivity and shifting T_{MIT}. In short, our experimental results show that replacing some La^{3+} with Nd^{3+} can adjust T_{MIT}.

Below T_{MIT}, resistivity ρ is observed to have ln$T$ dependence, as shown in Fig. 3(a). The local magnified image of the linear fitting is shown in Fig. S3 of SM, and the gray shaded area indicates the linear fitting range. The linear relationship of ρ–ln$T$ at low temperatures can commonly be attributed to three primary reasons: two-dimensional (2D) WL, Kondo scattering, and electron–electron interaction (EEI).[40–42] However, the response of these three effects varies significantly under magnetic field B. WL originates from the quantum interference effect, where the interference of two closed motion paths with time reversal symmetry is constructive, increasing the probability of electrons remaining at the origin. This interference can lead to the suppression of electronic diffusion, resulting in an increase in resistivity. Under the magnetic field, the time reversal symmetry is disrupted, resulting in quantum interference suppression. Therefore, as the magnetic field increases, WL will cause a decrease in resistance, resulting in negative MR.[43,44] The Kondo effect originates from spin-flip scattering between magnetic impurities and conduction electrons. At low temperatures, the interaction between electrons and antiferromagnetic impurities results in a rise in resistance.[42] A noteworthy aspect is that the antiferromagnetic interactions can be disrupted by magnetic fields. Therefore, the Kondo effect produces negative MR when the system is in a magnetic field, with magnetoresistance curves exhibiting a parabolic shape.[45] Due to the random distribution of magnetic impurities, the resistance of magnetic fields applied in different directions will not change significantly. As for EEI, it affects the density of states and therefore results in an isotropic and positive MR.[44–48]

To clarify the origin of the linear ρ–ln$T$ relationship at low temperatures, we performed MR measurements. As shown in Fig. 4, a significant negative out-of-plane magnetoresistance ($MR_\perp$) was observed for $La_{3-x}Nd_xNi_2O_7$ films (x = 0, 1.0, 1.5, 2.0, and 2.5). As previously elucidated, both the WL and Kondo scattering are capable of inducing negative MR. However, the precise mechanism that predominates in this phenomenon warrants further in-depth investigation and discussion.

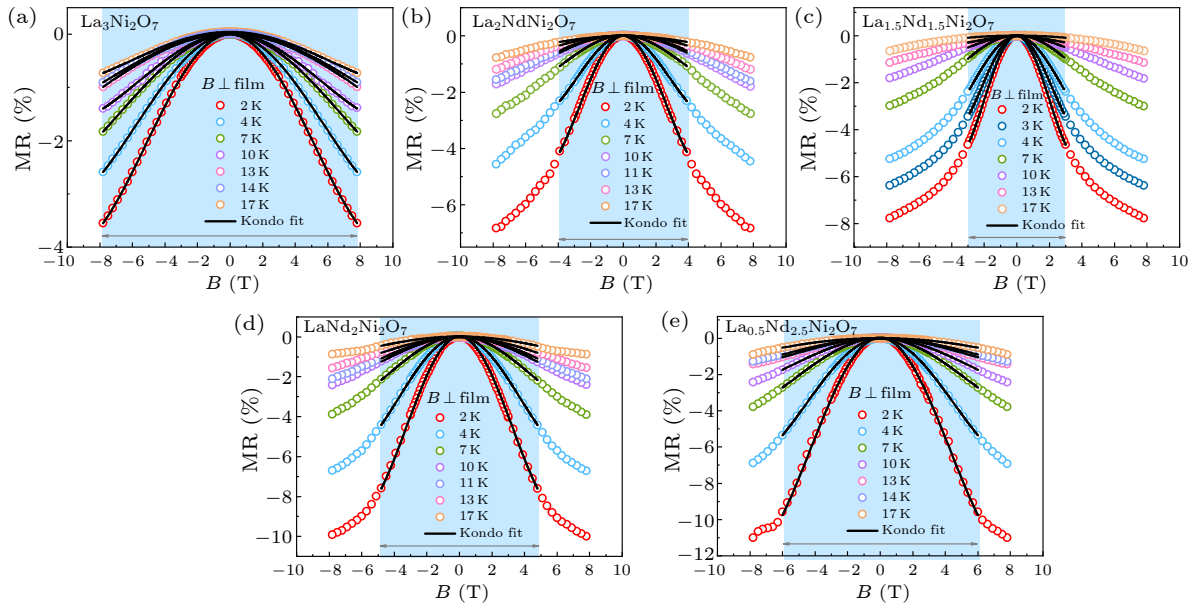

Fig. 4. Out-of-plane $MR_\perp$ for $La_{3-x}Nd_xNi_2O_7$ films with $x = 0, 1.0, 1.5, 2.0$, and 2.5 in (a)–(e), respectively. The black curves were fitted by Eq. (1) at temperatures of 2–17 K. The light blue areas represent the ranges of magnetic fields that can be well-fitted for all temperatures, which are (a) −7.8–7.8 T, (b) −3.9–3.9 T, (c) −3.0–3.0 T, (d) −4.8–4.8 T, and (e) −6.0–6.0 T, respectively.

3.1. Kondo Effect. To fit MR of our samples with the available theory, we use the Kondo model provided by Lee *et al.*,[49]

$$R^{\text{model}}(B) = R_0 + R_K\left(\frac{B}{B_1}\right), \tag{1}$$

$$R_K\left(\frac{B}{B_1}\right) = R_K(B=0)\cos^2\left[\frac{\pi}{2}M\left(\frac{B}{B_1}\right)\right], \tag{2}$$

where R_0 is the residual resistance, $R_K(B/B_1)$ is the general function of Kondo impurity MR at zero temperature, and B_1 is a magnetic scale related to both the Kondo temperature T_K and the g-factor of impurity spin.[44,50–52] $M(B/B_1)$ is provided in the SM.

As depicted in Fig. 4, the Kondo model provides excellent fits to the MR data across all doped samples at 2–17 K under varying fields, verifying the existence of Kondo scattering. Among them, the MR response of $La_3Ni_2O_7$ exhibits rigorous agreement with the Kondo model throughout the measured field range (±7.8 T). With the doping of Nd, the magnetic field range for Kondo model matching decreases initially and then increases, but does not surpass the range of $La_3Ni_2O_7$. When the doping concentration of Nd is 1.5, the minimum magnetic field range that can be fitted is only −3–3 T. The well-fitted range of magnetic fields is highlighted by the light blue area; for details, please see the Figs. S4 and S5 of SM. Combining the MR fitting range and ρ–T curves, we propose that the Kondo effect may exist and its contribution varies with the doping concentration, which is the greatest in the undoped sample $La_3Ni_2O_7$ and the least in the mid-doped $La_{1.5}Nd_{1.5}Ni_2O_7$.

3.2. 2D Weak Localization. To further determine the competitive relationship between Kondo and 2D WL in the $La_{3-x}Nd_xNi_2O_7$ (x = 0, 1.0, 1.5, 2.0, and 2.5) thin films, we conducted a fitting analysis on the conduction correction ($\Delta\sigma_{WL}$) for the samples. The WL contribution to conduction can be quantified using $\Delta\sigma_{WL}(B) = \sigma(B \neq 0) - \sigma(B = 0)$. We use the modified HLN formula[52–54] to fit $\Delta\sigma_{WL}$ calculated from $MR_\perp$ at the low field of 0–3 T,

$$\Delta\sigma_{WL}(B) = \frac{n\alpha e^2}{\pi h}\left[\Psi\left(\frac{1}{2}+\frac{B_\varphi}{B}\right) - \ln\frac{B_\varphi}{B}\right], \tag{3}$$

where Ψ is the digamma function, $B_\varphi = \hbar/4eD\tau_\varphi = \hbar/4el_\varphi^2$ is the dephasing field, D is the electronic diffusion constant, l_φ is the dephasing length, n is the number of parallel conductive channels ($n \approx 15$, considering that the c-axis lattice constant of a 15 nm thick bilayer nickelate film is approximately 2 nm[52]), and α is an effective parameter determined by magnetic scattering versus spin–orbit interaction (SOI). Usually, $\alpha = 1$ represents weak SOI and magnetic scattering, $\alpha = 0$ represents strong magnetic scattering, and $\alpha = -1/2$ represents strong SOI.

To enable a more consistent comparison across various doping levels, MR data at a normalized temperature of $0.1T_{MIT}$ were selected to perform the HLN fitting. The field-dependent conductance correction $\Delta\sigma_{WL}$ is plotted in Fig. 5(a), where the black solid curves are fitted from Eq. (3). It is obvious that the fitting curves match our experimental data very well. Figure 5(b) shows the variation of the fitting constant α with the doping concentration x. The α value in the $La_3Ni_2O_7$ (doping $x = 0$) film is close to 0, indicating strong magnetic scattering, suggesting that the Kondo effect dominates in the undoped $La_3Ni_2O_7$ film. As the Nd doping concentration x increases from 0 to 1.5, the α value gradually increases, indicating a weakening of the Kondo effect and an enhancement of 2D WL. Specifically, the α value increases close to 1 ($\alpha \approx 0.88$) in the $La_{1.5}Nd_{1.5}Ni_2O_7$ (doping $x = 1.5$) film, implying the

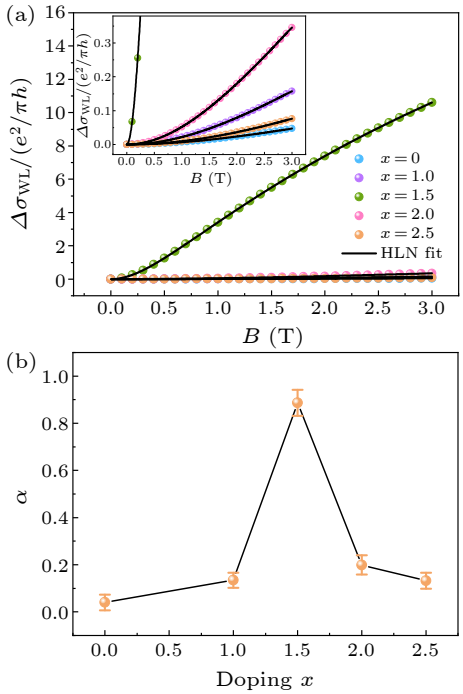

Fig. 5. (a) The conductance correction $\Delta\sigma_{WL}$ obtained from out-of-plane $MR_{\perp}$ for the $La_{3-x}Nd_xNi_2O_7$ films at the temperature of $0.1T_{MIT}$ (14 K for $x = 0, 2.5$, 11 K for $x = 1.0, 2.0$, and 3 K for $x = 1.5$, respectively). The black solid curves are fittings to the Eq. (3). The illustration shows the data and fitting curves at the low conduction-correction regime. (b) The variation of constant α extracted from HLN fitting with doping concentration x.

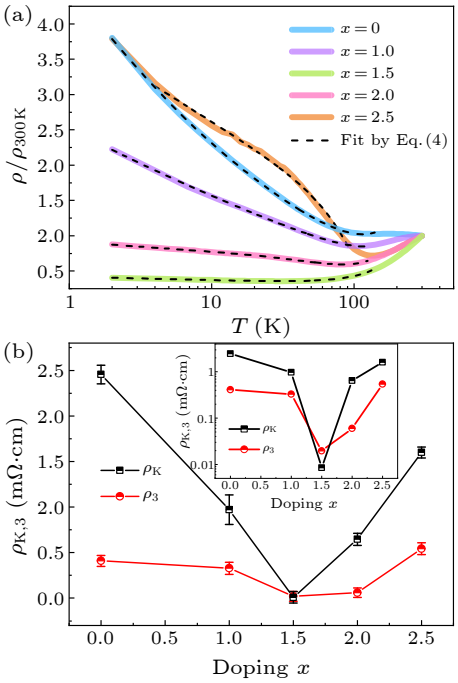

Fig. 6. (a) Normalized resistivity variation with temperature for the $La_{3-x}Nd_xNi_2O_7$ ($x = 0$, 1.0, 1.5, 2.0, and 2.5) films. The black dashed lines in (a) represent the fitting results based on the transport model described in Eq. (4). (b) The Kondo scattering term (ρ_K) and WL term (ρ_3) extracted from fits in (a) as a function of doping concentration x ($x = 0$, 1.0, 1.5, 2.0, and 2.5). Inset: ρ_K and ρ_3 (in logarithmic scale) versus doping concentration x ($x = 0$, 1.0, 1.5, 2.0, and 2.5).

main role of WL in this mid-doped sample. As for the $La_2NdNi_2O_7$ ($x = 1$), $LaNd_2Ni_2O_7$ ($x = 2$), and $La_{0.5}Nd_{2.5}Ni_2O_7$ ($x = 2.5$) films, although 2D WL is enhanced compared to the undoped $La_3Ni_2O_7$ film, the Kondo effect still dominates.

The previous results indicate a coexistence of the Kondo effect and the WL in the doped bilayer nickelate thin films. For a more comprehensive examination of transport characteristics and to quantify Kondo and WL effects in variably doped samples, we performed resistivity simulations incorporating various scattering mechanisms. We find that low-temperature resistivity behavior can be effectively described by a simple model including multiple scattering mechanisms,[36,55–59] and is given as

$$\rho(T) = \rho_0 + \rho_1 T^2 - \rho_3 \ln T + \rho_K \left[\frac{T^2}{T_K^2}(2^{1/s} - 1) + 1\right]^{-s}, \quad (4)$$

where ρ_0 is the residual resistivity. The T^2 term characterizes the dominant electron–electron interaction contribution to resistivity.[49] The ρ_K is the resistivity contributed by Kondo scattering,[57,58] and ρ_3 is the contribution of WL.[36] T_K is the Kondo temperature, and s ($s = 0.225$) is the impurity spin parameter.[36,59]

Below the T_{MIT}, the model fits well with the normalized resistivity, as shown in Fig. 6(a). Figure 6(b) depicts how the ρ_K and ρ_3 vary with the doping concentration x. From Fig. 6(b), as the Nd doping concentration x increases, both ρ_K and ρ_3 decrease first and then increase, which can well explain the changes in T_{MIT} as shown in Fig. 3(b). However, ρ_3 is relatively small and does not change significantly with doping, so the change in ρ_K plays a major role; that is, the variation of the Kondo effect during doping leads to changes in resistivity and MR. Except for the mid-doped sample with a doping concentration of $x = 1.5$ ($La_{1.5}Nd_{1.5}Ni_2O_7$ film), where ρ_3 is slightly greater than ρ_K [for clarity, see the inset of Fig. 6(b)]. The values of ρ_K in all other samples are greater than ρ_3. This result indicates that only in the mid-doped $La_{1.5}Nd_{1.5}Ni_2O_7$ film, the WL contribution is slightly higher than that of the Kondo effect, while the other samples are dominated by the Kondo effect, which aligns with the above analysis.

Although Nd/La substitution induces similar "chemical" pressure in the infinite-layer nickelates, both Nd-112 and La-112 phases show superconductivity with a unified phase diagram.[7] In other words, Nd/La substitution did not significantly alter the electronic structure and superconducting properties of 112-phase nickelate superconductors. For $La_{3-x}R_xNi_2O_7$ (R = La, Pr, Nd), however, recent investigations[39,60] reveal that smaller R^{3+} substitution not only reduces the lattice parameters (a, b, and c), but also generates significant orthorhombic distortions and c^+ octahedral rotations. Electronic correlation properties and electronic structure at the Fermi level in oxides are often strongly influenced by octahedral rotations.[61–63] Theoretical calculations[60] show that Nd will narrow the

bandwidth of Ni e_g orbitals ($3d_{x^2-y^2}$ and $3d_{z^2}$) at the Fermi level, leading to an increase in the band gap. Concurrently, there is an augmentation of the hybridization interaction between the Ni $3d_{x^2-y^2}$ orbitals and the basal O $2p_{x,y}$ orbitals, alongside a diminution of the hybridization interaction between Ni $3d_{z^2}$ and apical O $2p_z$. Notably, the density of states (DOS) at the Fermi level is largely conserved. This is in contrast to the effect of physical pressure, which broadens the bandwidth of the Ni e_g orbitals and causes the Ni $3d_{z^2}$ orbitals to rise through the Fermi level. Simultaneously, the DOS at the Fermi level increases, facilitating the transition to a superconducting state at a certain pressure. From this perspective, chemical pressure and physical pressure are two competing conditions. Therefore, doping with larger-radius cations [e.g., Sr^{2+} (1.44 Å), Ba^{2+} (1.61 Å)] offers an alternative chemical strategy.[64,65] Further research should help clarify the role of strain, Kondo effect, and WL that drive the MIT behavior in $La_3Ni_2O_7$ thin films, as well as obtaining possible full temperature metal states in strained thin films by tuning doping or growth conditions.

4. Conclusion. In summary, we have synthesized a series of $La_{3-x}Nd_xNi_2O_7$ ($x = 0$, 1.0, 1.5, 2.0, and 2.5) thin films on LAO substrates by PLD. The method of replacing part of La^{3+} with Nd^{3+} with a smaller radius did apply a certain compressive strain to the film, resulting in c-axis contraction with increasing doping concentration x. In addition, doping changed the transport properties of the film, and T_{MIT} decreased from 144 K of the undoped $La_3Ni_2O_7$ to 29 K of mid-doped $La_{1.5}Nd_{1.5}Ni_2O_7$. Finally, we obtained the variations and competitive relationship of the Kondo effect and the WL in thin films through theoretical analysis of the Kondo model, HLN fitting, and resistivity contribution model. As the doping level x rises, the contributions of the Kondo effect and the WL first decrease and then increase, which also explains to some extent the changes in T_{MIT}. Among them, the contribution of the WL is slightly higher than that of the Kondo effect only in the mid-doped $La_{1.5}Nd_{1.5}Ni_2O_7$, while the Kondo effect dominates in other $La_{3-x}Nd_xNi_2O_7$ ($x = 0$, 1.0, 2.0, and 2.5) samples. This result advances our comprehension of the physical mechanism of the MIT in bilayer nickelates.

Acknowledgements. This work was supported by the Natural Science Foundation of Guangdong Province of China (Grant No. 2025A1515011071), the National Natural Science Foundation of China (Grant Nos. 92065110, 11974048, and 12074334), and the Beijing Municipal Natural Science Foundation Key Research Topics (Grant No. Z230006).

References

[1] Bednorz J G and Müller K A 1986 *Z. Phys. B: Condens. Matter* **64** 189
[2] Hayward M A, Green M A, Rosseinsky M J, and Sloan J 1999 *J. Am. Chem. Soc.* **121** 8843
[3] Boris A V, Matiks Y, Benckiser E, Frano A, Popovich P, Hinkov V, Wochner P, Castro-Colin M, Detemple E, Malik V K, Bernhard C, Prokscha T, Suter A, Salman Z, Morenzoni E, Cristiani G, Habermeier H U, and Keimer B 2011 *Science* **332** 937
[4] Li D F, Lee K, Wang B Y, Osada M, Crossley S, Lee H R, Cui Y, Hikita Y, and Hwang H Y 2019 *Nature* **572** 624
[5] Osada M, Wang B Y, Goodge B H, Lee K, Yoon H, Sakuma K, Li D F, Miura M, Kourkoutis L F, and Hwang H Y 2020 *Nano Lett.* **20** 5735
[6] Osada M, Wang B Y, Lee K, Li D F, and Hwang H Y 2020 *Phys. Rev. Mater.* **4** 121801
[7] Osada M, Wang B Y, Goodge B H, Harvey S P, Lee K H, Li D F, Kourkoutis L F, and Hwang H Y 2021 *Adv. Mater.* **33** 2104083
[8] Pan G A, Segedin D F, LaBollita H, Song Q, Nica E M, Goodge B H, Pierce A T, Doyle S, Novakov S, Carrizales D C, N'Diaye A T, Shafer P, Paik H, Heron J T, Mason J A, Yacoby A, Kourkoutis L F, Erten O, Brooks C M, Botana A S, and Mundy J A 2022 *Nat. Mater.* **21** 160
[9] Li Q, He C P, Si J, Zhu X Y, Zhang Y, and Wen H H 2020 *Commun. Mater.* **1** 16
[10] Wang B X, Zheng H, Krivyakina E, Chmaissem O, Lopes P P, Lynn J W, Gallington L C, Ren Y, Rosenkranz S, Mitchell J F, and Phelan D 2020 *Phys. Rev. Mater.* **4** 084409
[11] Huo M W, Liu Z J, Sun H L, Li L S, Lui H, Huang C X, Liang F X, Shen B, and Wang M 2022 *Chin. Phys. B* **31** 107401
[12] Sun H L, Huo M W, Hu X W, Li J Y, Liu Z J, Han Y F, Tang L Y, Mao Z Q, Yang P T, Wang B S, Cheng J G, Yao D X, Zhang G M, and Wang M 2023 *Nature* **621** 493
[13] Zhang Y N, Su D J, Huang Y E, Shan Z Y, Sun H L, Huo M W, Ye K X, Zhang J W, Yang Z H, Xu Y K, Su Y, Li R, Smidman M, Wang M, Jiao L, and Yuan H Q 2024 *Nat. Phys.* **20** 1269
[14] Hou J, Yang P T, Liu Z Y, Li J Y, Shan P F, Ma L, Wang G, Wang N N, Guo H Z, Sun J P, Uwatoko Y, Wang M, Zhang G M, Wang B S, and Cheng J G 2023 *Chin. Phys. Lett.* **40** 117302
[15] Wang G, Wang N N, Shen X L, Hou J, Ma L, Shi L F, Ren Z A, Gu Y D, Ma H M, Yang P T, Liu Z Y, Guo H Z, Sun J P, Zhang G M, Calder S, Yan J Q, Wang B S, Uwatoko Y, and Cheng J G 2024 *Phys. Rev. X* **14** 011040
[16] Zhou Y Z, Guo J, Cai S, Sun H L, Li C Y, Zhao J Y, Wang P Y, Han J Y, Chen X T, Chen Y J, Wu Q, Ding Y, Xiang T, Mao H K, and Sun L L 2025 *Matter Radiat. Extrem.* **10** 027801
[17] Wang N N, Wang G, Shen X L, Hou J, Luo J, Ma X P, Yang H X, Shi L F, Dou J, Feng J, Yang J, Shi Y Q, Ren Z A, Ma H M, Yang P T, Liu Z Y, Liu Y, Zhang H, Dong X L, Wang Y X, Jiang K, Hu J P, Nagasaki S, Kitagawa K, Calder S, Yan J Q, Sun J P, Wang B S, Zhou R, Uwatoko Y, and Cheng J G 2024 *Nature* **634** 579
[18] Li Q, Zhang Y J, Xiang Z N, Zhang Y H, Zhu X Y, and Wen H H 2024 *Chin. Phys. Lett.* **41** 017401
[19] Sakakibara H, Ochi M, Nagata H, Ueki Y, Sakurai H, Matsumoto R, Terashima K, Hirose K, Ohta H, Kato M, Takano Y, and Kuroki K 2024 *Phys. Rev. B* **109** 144511
[20] Zhu Y H, Peng D, Zhang E K, Pan B Y, Chen X, Chen L X, Ren H F, Liu F Y, Hao Y Q, Li N A, Xing Z F, Lan F J, Han J Y, Wang J J, Jia D H, Wo H L, Gu Y Q, Gu Y M, Ji L, Wang W B, Gou H Y, Shen Y, Ying T P, Chen X L, Yang W E, Cao H B, Zheng C L, Zeng Q S, Guo J G, and Zhao J 2024 *Nature* **631** 531
[21] Huang J K and Zhou T 2024 *Phys. Rev. B* **110** L060506
[22] Nagata H, Sakurai H, Ueki Y, Yamane K, Matsumoto R, Terashima K, Hirose K, Ohta H, Kato M, and Takano Y 2024 *J. Phys. Soc. Jpn.* **93** 095003
[23] Souliou S M, Gretarsson H, Garbarino G, Bosak A, Porras J, Loew T, Keimer B, and Le Tacon M 2018 *Phys. Rev. B* **97** 020503

[24] Cyr-Choinière O, LeBoeuf D, Badoux S, Dufour-Beauséjour S, Bonn D A, Hardy W N, Liang R, Graf D, Doiron-Leyraud N, and Taillefer L 2018 *Phys. Rev. B* **98** 064513

[25] Chen X Y, Choi J, Jiang Z C, Mei J, Jiang K, Li J, Agrestini S, Garcia-Fernandez M, Sun H L, Huang X, Shen D W, Wang M, Hu J P, Lu Y, Zhou K J, and Feng D L 2024 *Nat. Commun.* **15** 10522

[26] Li Z, Guo W, Zhang T T, Song J H, Gao T Y, Gu Z B, and Nie Y F 2020 *APL Mater.* **8** 091112

[27] Liu Y C, Ou M J, Chu H F, Yang H, Li Q, Zhang Y J, and Wen H H 2024 *Phys. Rev. Mater.* **8** 124801

[28] Ko E K, Yu Y J, Liu Y D, Bhatt L, Li J R, Thampy V, Kuo C T, Wang B Y, Lee Y, Lee K, Lee J S, Goodge B H, Muller D A, and Hwang H Y 2025 *Nature* **638** 935

[29] Zhou G D, Lv W, Wang H, Nie Z H, Chen Y Q, Li Y Y, Huang H L, Chen W Q, Sun Y J, Xue Q K, and Chen Z Y 2025 *Nature* **640** 641

[30] van der Pauw L J 1991 *Semicond. Dev.: Pioneering Papers.* p. 174

[31] Nie J C, Yamasaki H, and Mawatari Y 2004 *Phys. Rev. B* **70** 195421

[32] Wang L, Chang L, Yin X M, Rusydi A, You L, Zhou Y, Fang L, and Wang J L 2017 *J. Phys.: Condens. Matter* **29** 025002

[33] Ling C D, Argyriou D N, Wu G Q, and Neumeier J J 2000 *J. Solid State Chem.* **152** 517

[34] Wu K T, Soh Y A, and Skinner S J 2013 *Mater. Res. Bull.* **48** 3783

[35] Bagués N, Santiso J, Esser B D, Williams R E A, McComb D W, Konstantinovic Z, Balcells L, and Sandiumenge F 2018 *Adv. Funct. Mater.* **28** 1704437

[36] Rimal G, Tasnim T, Ortiz G C, Sterbinsky G E, Hwang J, and Comes R B 2024 *Phys. Rev. Mater.* **8** L071201

[37] Muraoka Y and Hiroi Z 2002 *Appl. Phys. Lett.* **80** 583

[38] Nagashima K, Yanagida T, Tanaka H, and Kawai T 2006 *J. Appl. Phys.* **100** 063714

[39] Wang G, Wang N N, Lu T L, Calder S, Yan J Q, Shi L F, Hou J, Ma L, Zhang L L, Sun J P, Wang B S, Meng S, Liu M, and Cheng J G 2025 *npj Quantum Mater.* **10** 1

[40] Lee P A and Ramakrishnan T V 1985 *Rev. Mod. Phys.* **57** 287

[41] Altshuler B L and Aronov A G 1983 *Solid State Commun.* **46** 429

[42] Kondo J 1964 *Prog. Theor. Phys.* **32** 37

[43] Wang S G and Lindelof P E 1988 *J. Low Temp. Phys.* **71** 403

[44] Das S, Rastogi A, Wu L J, Zheng J C, Hossain Z, Zhu Y M, and Budhani R C 2014 *Phys. Rev. B* **90** 081107

[45] Xue H X, Hong Y P, Li C J, Meng J C, Li Y C, Liu K J, Liu M R, Jiang W M, Zhang Z, He L, Dou R F, Xiong C M, and Nie J C 2018 *Phys. Rev. B* **98** 085305

[46] Kumar P, Dogra A, Bhadauria P P S, Gupta A, Maurya K K, and Budhani R C 2015 *J. Phys.: Condens. Matter* **27** 125007

[47] Zhang S X, Ogale S B, Yu W Q, Gao X Y, Liu T, Ghosh S, Das G P, Wee A T S, Greene R L, and Venkatesan T 2009 *Adv. Mater.* **21** 2282

[48] Wang J, DaSilva A M, Chang C Z, He K, Jain J K, Samarth N, Ma X C, Xue Q K, and Chan M H W 2011 *Phys. Rev. B* **83** 245438

[49] Lee M, Williams J R, Zhang S P, Frisbie C D, and Goldhaber-Gordon D 2011 *Phys. Rev. Lett.* **107** 256601

[50] Andrei N, Furuya K, and Lowenstein J H 1983 *Rev. Mod. Phys.* **55** 331

[51] Shao T N, Zhang Z T, Qiao Y J, Zhao Q, Liu H W, Chen X X, Jiang W M, Yao C L, Chen X Y, Chen M H, Dou R F, Xiong C M, Zhang G M, Yang Y F, and Nie J C 2023 *Natl. Sci. Rev.* **10** nwad112

[52] Wang X Y, Chen M H, Chen C X, Zhao Q, Zhu F H, Yang W L, Chen X Y, Yan M L, Dou R F, Xiong C M, and Nie J C 2025 *Phys. Rev. B* **111** 094506

[53] Liao J, Ou Y B, Liu H W, He K, Ma X C, Xue Q K, and Li Y Q 2017 *Nat. Commun.* **8** 16071

[54] Hikami S, Larkin A I, and Nagaoka Y 1980 *Prog. Theor. Phys.* **63** 707

[55] Jiang W M, Zhao Q, Zhang Z, Shao T N, Zhang Z T, Liu M R, Yao C L, Qiao Y J, Chen M H, Chen X Y, Dou R F, Xiong C M, and Nie J C 2023 *Solid State Commun.* **366** 115154

[56] Costi T A, Hewson A C, and Zlatic V 1994 *J. Phys.: Condens. Matter* **6** 2519

[57] Goldhaber-Gordon D, Göres J, Kastner M A, Shtrikman H, Mahalu D, and Meirav U 1998 *Phys. Rev. Lett.* **81** 5225

[58] Cai X X, Yue J, Xu P, Jalan B, and Pribiag V S 2021 *Phys. Rev. B* **103** 115434

[59] Choudhary R, Nair S, Yang Z F, Lee D, and Jalan B 2022 *APL Mater.* **10** 091118

[60] Geisler B, Hamlin J J, Stewart G R, Hennig R G, and Hirschfeld P J 2024 *npj Quantum Mater.* **9** 38

[61] Hu B, McCandless G T, Garlea V O, Stadler S, Xiong Y M, Chan J Y, Plummer E W, and Jin R 2011 *Phys. Rev. B* **84** 174411

[62] Mesa D, Ye F, Chi S X, Fernandez-Baca J A, Tian W, Hu B A, Jin R, Plummer E W, and Zhang J D 2012 *Phys. Rev. B* **85** 180410

[63] Nakayama M, Kondo T, Kuroda K, Bareille C, Watson M D, Kunisada S, Noguchi R, Kim T K, Hoesch M, Yoshida Y, and Shin S 2018 *Phys. Rev. B* **98** 161102

[64] Jiao K K, Niu R, Xu H X, Zhen W L, Wang J R, and Zhang C J 2024 *Physica C* **621** 1354504

[65] Xu M Y, Huyan S, Wang H Z, Bud'ko S L, Chen X L, Ke X L, Mitchell J F, Canfield P C, Li J, and Xie W W 2024 *Adv. Electron. Mater.* **10** 202400078